

# How well can we reconstruct the $t\bar{t}$ system near its threshold at future $e^+e^-$ linear colliders?

K. Ikematsu<sup>1,a</sup>, K. Fujii<sup>2,b</sup>, Z. Hioki<sup>3,c</sup>, Y. Sumino<sup>4,d</sup>, T. Takahashi<sup>5,e</sup>

<sup>1</sup> Department of Physics, Hiroshima University, Higashi Hiroshima 739-8526, Japan

<sup>2</sup> IPNS, KEK, Tsukuba 305-0801, Japan

<sup>3</sup> Institute of Theoretical Physics, University of Tokushima, Tokushima 770-8502, Japan

<sup>4</sup> Department of Physics, Tohoku University, Sendai 980-8578, Japan

<sup>5</sup> Graduate School of Advanced Sciences of Matter, Hiroshima University, Higashi Hiroshima 739-8530, Japan

Received: 4 March 2003 /

Published online: 23 May 2003 – © Springer-Verlag / Società Italiana di Fisica 2003

**Abstract.** We developed a new method for the full kinematical reconstruction of the  $t\bar{t}$  system near its threshold at future linear  $e^+e^-$  colliders. In the core of the method lies likelihood fitting which is designed to improve measurement accuracies of the kinematical variables that specify the final states resulting from  $t\bar{t}$  decays. The improvement is demonstrated by applying this method to a Monte Carlo  $t\bar{t}$  sample generated with various experimental effects including beamstrahlung, finite acceptance and resolution of the detector system, etc. In most cases the fit takes a broad non-Gaussian distribution of a given kinematical variable to a nearly Gaussian shape, thereby justifying phenomenological analyses based on simple Gaussian smearing of the parton-level momenta. The standard deviations of the resultant distributions of various kinematical variables are given in order to facilitate such phenomenological analyses. A possible application of the kinematical fitting method and its expected impact are also discussed.

## 1 Introduction

The discovery of the top quark [1] at Tevatron has completed the standard-model (SM) list of matter fermions. In spite of subsequent studies, our knowledge on its properties is still far below the level we reached for the lighter matter fermions. A next-generation  $e^+e^-$  linear collider such as JLC [2], having a facet as a top-quark factory, is expected to allow us to measure the top-quark's properties with unprecedented precision, thereby improving this situation dramatically. Such precision measurements may shed light on the electroweak-symmetry-breaking mechanism or hint at physics beyond the SM, or both.

Being aware of the opportunities provided by the linear collider, a number of authors have so far performed interesting analyses of the measurements of top-quark properties [3–6]. They can be classified into two categories, i.e., those near the  $t\bar{t}$  threshold, mainly focused on physics contained in the threshold enhancement factor, and those in the open-top region, searching for anomalies in production and decay vertices, both of which play important roles and complement each other.

In those analyses, feasibility studies on form factor measurements have been done mainly in the open-top region [7–9]. In the meantime, it has been conceived that, in view of the energy upgrading scenario of the  $e^+e^-$  linear collider, measurements of the top form factors in the  $t\bar{t}$  threshold region are also important. The top-quark physics is expected to commence in the threshold region at the early stage of the collider operation and a full exploration of the machine's potential in that phase is crucial for the design of the project. It has, therefore, repeatedly been stressed that a realistic simulation study is desperately needed to clarify the feasibility of precision measurements of the form factors at the  $t\bar{t}$  threshold. Besides, form factor measurements in the  $t\bar{t}$  threshold region have some favorable features: the availability of a well-controlled highly polarized top sample [10,11]; no need for transformation to  $t$  or  $\bar{t}$  rest frames because both  $t$  and  $\bar{t}$  are nearly at rest; and as far as the decay form factor measurements of an on-shell top quark are concerned, the center-of-mass energy does not matter.

In order to thoroughly carry out such analyses for real data, we need a sophisticated method to kinematically reconstruct events as efficiently and as precisely as possible. This is, however, highly non-trivial in practice, due to finite detector resolutions, possible missing neutrinos in the final states, and various background contributions. Furthermore, care has to be taken when imposing a kinematical constraint on the masses of the  $t$  and  $\bar{t}$  quarks

<sup>a</sup> e-mail: ikematsu@post.kek.jp

<sup>b</sup> e-mail: fujiik@jlcf.kek.jp

<sup>c</sup> e-mail: hioki@ias.tokushima-u.ac.jp

<sup>d</sup> e-mail: sumino@tuhep.phys.tohoku.ac.jp

<sup>e</sup> e-mail: tohrut@hiroshima-u.ac.jp

because they cannot be simultaneously on-shell below the threshold. We thus need to further explore the potential of the  $e^+e^-$  linear collider and extend the past studies [7, 8, 12, 13] to the threshold region, in order to make maximum use of the linear collider’s advantages: a clean experimental environment, a well-defined initial state, the availability of a highly polarized electron beam, the possibility of a full parton-level reconstruction of the final states, etc.

In this paper, we thus aim at developing an efficient method for the full kinematical reconstruction of the  $t\bar{t}$  system near its threshold in  $e^+e^-$  annihilation and clarifying the accuracy to which various observables will be measured. We develop a likelihood fitting method which is especially designed to improve measurement accuracies of the kinematical variables of the particles originating from the  $t\bar{t}$  sample in the threshold region. Moreover, some of the analysis techniques developed here are expected to be useful for the analyses in the open-top region.

Our study should also provide important information to the current line of phenomenological studies on top-quark physics at linear colliders. In fact, there have been a number of theoretical studies on measurements of the top-quark production and decay form factors using the  $e^+e^- \rightarrow t\bar{t}$  process [3–6]. However, many of these analyses assumed either the most optimistic case or the most conservative case with respect to the kinematical reconstruction of event profiles. In the former case, one assumes that the momenta of all the particles (including  $t$  and  $W$ ) can be determined precisely, while in the latter case one uses only partial kinematical information, e.g. the direction of  $b$ , and the energy and momentum of  $\ell$ . In this work we will provide realistic values of resolutions with which individual kinematical variables can be measured.

In Sect. 2 we briefly review our simulation framework. Section 3 is devoted to top-quark reconstruction in the lepton-plus-4-jet mode, where two subsections recapitulate the basic strategy and procedure, respectively. In Sect. 4 we explain our kinematical reconstruction using a likelihood fitting method. Then we discuss a possible application of this method and its expected impact in Sect. 5. Finally, Sect. 6 summarizes our results and concludes this paper.

## 2 Framework of analysis

For Monte Carlo-simulation studies of  $t\bar{t}$  productions and decays, we developed an event generator that is now included in physsim-2001a [14], where the amplitude calculation and phase space integration are performed with HELAS/BASES [15, 16] and parton 4-momenta of an event are generated by SPRING [16]. In the amplitude calculation, initial-state radiation (ISR) as well as  $S$ - and  $P$ -wave QCD corrections to the  $t\bar{t}$  system [17, 18] are taken into account. Parton showering and hadronization are carried out using JETSET 7.4 [19] with final-state tau leptons treated by TAUOLA [20] in order to handle their polarizations properly.

In this study, the top-quark (pole) mass is assumed to be 175 GeV and the nominal center-of-mass energy is set

**Table 1.** ACFA study parameters of the JLC detector, where  $p$ ,  $p_T$ , and  $E$  are measured in units of GeV

| Detector              | Performance  | Coverage                  |
|-----------------------|--|---------------------------|
| Vertex detector       | $\sigma_b = 7.0 \oplus (20.0/p) / \sin^{3/2} \theta \mu\text{m}$ | $ \cos \theta  \leq 0.90$ |
| Central drift chamber | $\sigma_{p_T}/p_T = 1.1 \times 10^{-4} p_T \oplus 0.1\%$         | $ \cos \theta  \leq 0.95$ |
| EM calorimeter        | $\sigma_E/E = 15\% / \sqrt{E} \oplus 1\%$                        | $ \cos \theta  \leq 0.90$ |
| Hadron calorimeter    | $\sigma_E/E = 40\% / \sqrt{E} \oplus 2\%$                        | $ \cos \theta  \leq 0.90$ |

at 2 GeV above the  $1S$  resonance of the  $t\bar{t}$  bound states. This energy is known to be suitable for measurements of various properties of the  $t\bar{t}$  system at threshold [12]. We will assume an electron-beam polarization of 80% in what follows. Effects of natural beam-energy spread and beamstrahlung are taken into account according to the prescription given in [12], where the details of the beam parameters are also described. We have assumed no crossing angle between the electron and the positron beams and ignored the transverse component of the initial-state radiation. Consequently, the  $t\bar{t}$  system in our Monte Carlo sample has no transverse momentum. Under these conditions we expect 40 k  $t\bar{t}$  events for  $100 \text{ fb}^{-1}$ .

The generated Monte Carlo  $t\bar{t}$  events were passed to a detector simulator (JSF Quick Simulator [21]) which incorporates the ACFA-JLC study parameters (see Table 1). The quick simulator created vertex-detector hits, smeared charged-track parameters in the central tracker with the parameter correlation properly taken into account, and simulated calorimeter signals as from individual segments, thereby allowing for a realistic simulation of cluster overlapping. It should also be noted that track-cluster matching was performed to achieve the best energy-flow measurements.

## 3 Event selection

### 3.1 Basic reconstruction strategy

Since the top quark decays for almost 100% into a  $b$  quark and a  $W$  boson, the signature of  $t\bar{t}$  production is two  $b$  jets and two  $W$  bosons in the final state. These  $W$  bosons decay subsequently either leptonically into a lepton plus a neutrino or hadronically into two jets. According to how the  $W$  bosons decay, therefore, there will be three modes of final states:

- (1) six jets, where both of the  $W$ s decay hadronically,
- (2) one lepton plus four jets, where one of the  $W$ ’s decays leptonically and the other hadronically, and
- (3) two leptons plus two jets, where both of the  $W$ s decay leptonically.

In order to reconstruct the momentum vector of the top quark, we will use the lepton-plus-4-jet mode, for which we can reconstruct the  $t$  ( $\bar{t}$ )-quark momentum as the momentum sum of the  $b$  ( $\bar{b}$ ) jet and the two jets from the hadronically decayed  $W^+$  ( $W^-$ ), while we can tell the

charge of the hadronically decayed  $W$  from the charge of the lepton.

In the lepton-plus-4-jet mode, two of the four jets are  $b$  ( $\bar{b}$ ) jets directly from the  $t$  ( $\bar{t}$ ) quarks, while the other two are from the  $W$  boson that decayed hadronically. Therefore, if one can identify the  $b$  and  $\bar{b}$  jets, the remaining two jets can be uniquely assigned as decay products of the  $W$  boson. The other  $W$  boson can be reconstructed from the lepton and the neutrino indirectly detected as a missing momentum. The remaining task is then to decide which  $b$  ( $\bar{b}$ ) jet to attach to which  $W$ -boson candidate, in order to form  $t$  ( $\bar{t}$ ) quarks. Since the  $t$  ( $\bar{t}$ ) quarks are virtually at rest near the threshold, a  $b$  ( $\bar{b}$ ) jet and the corresponding  $W$  boson fly in the opposite directions. We can thus choose the correct combination by requiring the  $b$  ( $\bar{b}$ ) jet and the  $W$  boson to be approximately back-to-back.

In reality, however,  $b$  ( $\bar{b}$ )-quark tagging is not perfect and can be performed only with some finite efficiency and purity: there could be more than two  $b$  ( $\bar{b}$ )-jet candidates in a single event. In addition,  $b$  and  $\bar{b}$  quarks can be emitted in the same direction. In such a case, a wrong combination could accidentally satisfy the back-to-back condition. These facts sometimes prevent us from uniquely assigning each jet to its corresponding parton, resulting in multiple solutions for a single event. Moreover, the leptonically decayed  $W$  is poorly reconstructed in practice, since the neutrino momentum is strongly affected by ISR, beamstrahlung, as well as other possible neutrinos emitted from the  $b$  ( $\bar{b}$ ) jets. In order to overcome these difficulties, we will need some sophisticated method. We defer discussion of such a method to the next section and examine here the extent to which the aforementioned basic reconstruction strategy works.

### 3.2 Event selection procedure

The lepton-plus-4-jet-mode selection started with demanding an energetic isolated lepton:  $E_\ell > 18$  GeV and  $E_{14^\circ\text{cone}} < 18$  GeV, where  $E_\ell$  is the lepton's energy and  $E_{14^\circ\text{cone}}$  is the energy sum of particles within a cone with a half angle of  $14^\circ$  around the lepton direction excluding the lepton itself.<sup>1</sup> When such a lepton was found, the rest of the final-state particles was forced to clustering to four jets, using the Durham clustering algorithm [22]. The two-jet invariant mass was then calculated for each of the six possible combinations and it was checked if it was between 65 GeV and 95 GeV, in order to select a jet pair which was consistent with that coming from a  $W$ -boson decay. For such a jet pair the remaining two jets, at the same time, had to be identified as  $b$  ( $\bar{b}$ ) jets, using flavor tagging based on the impact parameter method. The hatched histogram in Fig. 1 is the 2-jet invariant mass distribution of all the possible pairs out of the four jets, the solid histogram being that with the  $b$ -tagging. It is seen that this procedure

<sup>1</sup> The  $E_\ell$  cut was chosen to be the kinematical limit for the lepton from the  $W \rightarrow \ell\nu$  decay. On the other hand, the cone-energy cut was optimized to achieve high purity, while keeping a reasonable efficiency

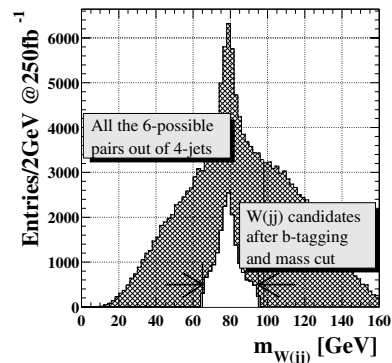


**Fig. 1.** Invariant mass distributions of the 2-jet systems reconstructed as  $W$ -boson candidates. Hatched and solid histograms correspond to before and after double  $b$ -tagging, respectively. The locations of the  $W$  mass cuts are indicated with arrows

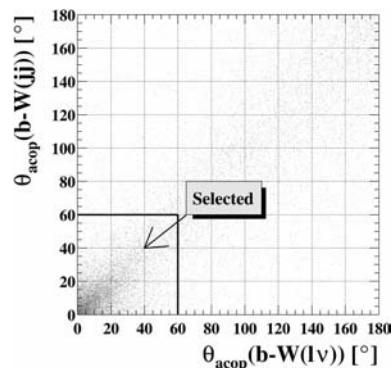


**Fig. 2.** Scatter plot of the acoplanarity angles corresponding to two  $b$ - $W$  systems, where horizontal and vertical axes are angles of  $b$ - $W_{\ell\nu}$  and  $b$ - $W_{2\text{-jet}}$  systems, respectively

dramatically improved the purity of the  $W$ -boson sample. It should also be stressed that these selection criteria are very effective to suppress background processes such as  $e^+e^- \rightarrow W^+W^-$  and provide us with an essentially background-free  $t\bar{t}$  event sample.

The remaining task is to decide which  $b$  ( $\bar{b}$ ) jet to associate with which  $W$  candidate. For a  $b$  ( $\bar{b}$ )-jet candidate, the right  $W$ -boson partner was selected by requiring the back-to-back condition as described above. Figure 2 is a scatter plot of the acoplanarity angles of the two possible  $b$ - $W$  systems, where horizontal and vertical axes are the angles of  $b$ - $W_{\ell\nu}$  and  $b$ - $W_{2\text{-jet}}$  system, respectively.  $b$ - $W$  pairs having  $\theta_{\text{acop}(b-W)} \leq 60^\circ$  were regarded as daughters of the  $t$  ( $\bar{t}$ ) quarks.

The selection efficiency after all of these cuts was found to be 15% including the branching fraction to the lepton-plus-4-jet mode of 29%.

## 4 Kinematical fit

The event selection described above yields a very clean  $t\bar{t}$  sample. As noted above, however, the sample is still subject to combinatorial backgrounds, if we are to fully reconstruct the final state by assigning each jet to a cor-

responding decay daughter of the  $t$  or  $\bar{t}$  quark. We thus need a well-defined criterion to select the best from the possible multiple solutions. It is also desirable to improve the measurement accuracies of those kinematical variables which are suffering from the effects of missing neutrinos (such variables include the momenta of  $b$ ,  $\bar{b}$  or the neutrino from a  $W$  itself).

The  $t\bar{t}$  system produced via  $e^+e^-$  annihilation is a heavily constrained system: there are many mass constraints in addition to the usual 4-momentum conservation. At  $e^+e^-$  linear colliders, thanks to their well-defined initial state and the clean environment, we can make full use of these constraints and perform a kinematical fit to select the best solution and to improve the measurement accuracies of the kinematical variables of the final-state partons.

#### 4.1 Parameters, constraints, and likelihood function

For the lepton-plus-4-jet final state, there are ten unknown parameters to be determined by the fit: the energies of four jets, the 4-momentum of the neutrino from the leptonically decayed  $W$  boson, and the energies of the initial-state electron and positron, provided that the jet directions as output from the jet finder are accurate enough, the error in the 4-momentum measurement of the lepton from the leptonically decayed  $W$  can be ignored, and that the transverse momenta of the initial-state electron and positron after beamstrahlung or initial-state radiation or both are either negligible or are known from a low angle  $e^+/e^-$  detector system<sup>2</sup> (see Fig. 3).

The requirements of 4-momentum conservation and the massless constraint for the neutrino from the leptonically decayed  $W$  reduce the number of free parameters to five. We choose as these free parameters the energies of the four jets and the initial longitudinal momentum (the difference of the energies of the initial-state electron and positron).

These five unknown parameters can be determined by maximizing the following likelihood function:

$$L = \left( \prod_{f=1}^4 P_{E_f}^f(E_f^{\text{measured}}, E_f) \right) \cdot P_{\Gamma_{W^+}} \cdot P_{\Gamma_{W^-}} \cdot P_{\Gamma_{t\bar{t}}} \cdot P_{\sqrt{s}}, \quad (1)$$

where  $P_{E_f}^f$  is a resolution function for jet  $f$  and is Gaussian for  $f = 1$  and 2 (jets from the hadronically decayed  $W$ ) as given by the detector energy resolution. For  $f = 3$  and 4 (jets from the  $b$  and  $\bar{b}$  quarks) the resolution function is the same Gaussian convoluted with the missing energy spectrum due to possible neutrino emissions. For the two  $W$  bosons in the final state, we use a Breit–Wigner function  $P_{\Gamma_W}$  instead of  $\delta$ -function-like mass constraints.  $P_{\sqrt{s}}$

<sup>2</sup> In addition, there will be some finite transverse momenta due to a finite crossing angle of the two beams. These transverse momenta are, however, known and can easily be incorporated into the fit

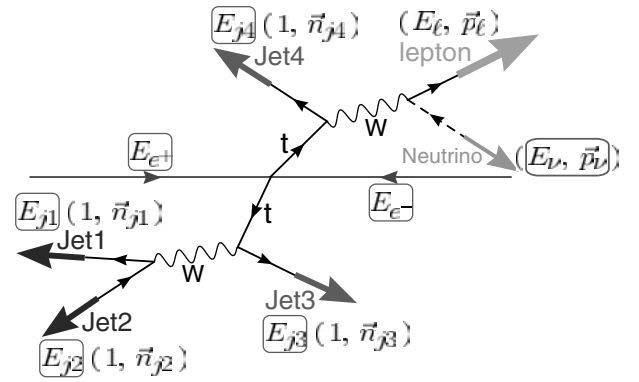


**Fig. 3.** Schematic diagram showing parameters and constraints relevant to the kinematical fit described in the text. The boxed parameters are unknown and are to be determined by the fit

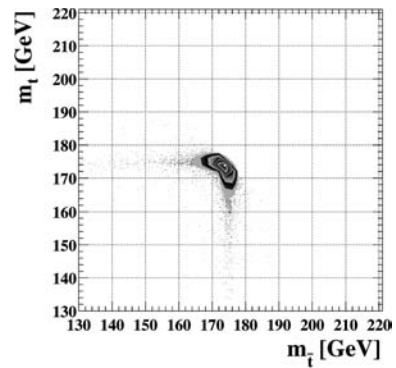


**Fig. 4.**  $P_{\Gamma_{t\bar{t}}}$  distribution below  $t\bar{t}$  threshold

is a weight function coming from ISR and beamstrahlung effects. This distribution was calculated as a differential cross section as a function of the energies of initial-state electron and positron, taking into account the  $t\bar{t}$  threshold correction as described in Sect. 2.

The remaining factor,  $P_{\Gamma_{t\bar{t}}}$ , controls the mass distribution of the  $t$  and  $\bar{t}$  quarks and has been introduced to take into account the kinematical constraint that the  $t$  and  $\bar{t}$  cannot be simultaneously on-shell below threshold (see Fig. 4, which shows the  $P_{\Gamma_{t\bar{t}}}$  distribution below  $t\bar{t}$  threshold). The  $P_{\Gamma_{t\bar{t}}}$  distribution is a dynamics-independent factor which is extracted from the theoretical formula for the threshold cross section.

#### 4.2 Results

We performed the maximum likelihood fit for the selected sample. The maximum likelihood fit provided us with a well-defined clear-cut criterion to select the best solution, when there were multiple possible solutions for a single event: we should select the one with the highest likelihood.

Figure 5a,b is the reconstructed  $W$ -mass distributions for the leptonically and hadronically decayed  $W$  bosons, respectively, before (hatched) and after (solid) the kinematical fit. The figures demonstrate that the Breit–Wigner

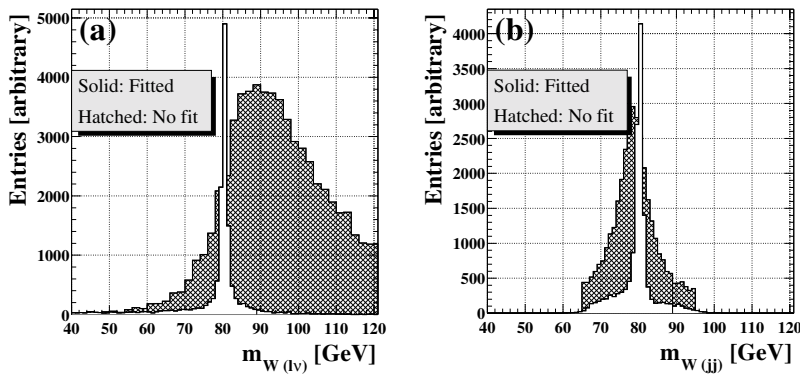


**Fig. 5a,b.** Reconstructed  $W$ -mass distributions for **a** leptonically and **b** hadronically decayed  $W$  bosons, before (*hatched*) and after (*solid*) the kinematical fitting. Note that the vertical scale for the hatched area is enhanced by a factor of five for illustration purposes

factors ( $P_{\Gamma_{W^\pm}}$ ) in the likelihood function properly constrain the  $W$  masses as intended.

Figure 6a plots the reconstructed mass for the  $t$  ( $\bar{t}$ ) decayed into three jets against that of the  $\bar{t}$  ( $t$ ) decayed into a lepton plus a  $b$  jet, before the kinematical fit. The strong negative correlation is due to the fact that the neutrino from the leptonically decayed  $W$  is reconstructed as the total missing momentum. Figure 6b,c is the projections of Fig. 6a to the horizontal and vertical axes, respectively, showing systematic shifts of the peak positions.<sup>3</sup> Figure 6d–f shows plots similar to Fig. 6a–c after the kinematical fitting, while Fig. 6g–i shows the corresponding distributions of generated values (Monte Carlo truth). The kinematical fit sent most of the events to the L-shaped region indicated in Fig. 6d, as it should, and made the distribution look like the generated distribution shown in Fig. 6g. Consequently, the peak shifts observed in the Fig. 6b,c have been corrected as seen in Fig. 6e,f. There is, however, still some small fraction of events left along the minus  $45^\circ$  line. These events were so poorly measured that it was impossible to restore. The cut (angled region) indicated in Fig. 6d allowed us to remove them without introducing any strong bias on the reconstruction of the kinematical variables.

Now the question is how the above constraints improve the parameters of the fit such as the energies of the  $b$  and  $\bar{b}$  jets, the direction and the magnitude of the missing neutrino from the leptonically decayed  $W$ , on which we expect significant influences. Figure 7a,b plots the difference between the reconstructed and the generated energies of the  $b$  ( $\bar{b}$ ) quark attached to the leptonically decayed  $W$  and that of the  $\bar{b}$  ( $b$ ) attached to the hadronically decayed  $W$ , respectively, before (*hatched*) and after (*solid*) the kinematical fit. The plots demonstrate that the kinematical constraints recover the energies carried away by neutrinos from the  $b$  or  $\bar{b}$  decays. The kinematical fit takes broad non-Gaussian distributions into nearly Gaussian shapes. The standard deviations of the  $b$  or  $\bar{b}$  jet-energy distri-

butions are approximately 3.5 GeV after the kinematical fit.

The improvement is more dramatic for the direct neutrino from the leptonically decayed  $W$ , which is reconstructed as the total missing momentum; see Fig. 7c,d, which shows the distributions of the difference of the reconstructed and generated neutrino energies ( $\Delta E_\nu$ ) and directions ( $\Delta\theta_\nu$ ). Again the kinematical fit makes the broad and skewed distribution of neutrino energies have a nearly Gaussian shape with a standard deviation of approximately 2.5 GeV. The fit also improves the angular resolution as shown in Fig. 7d. The resultant angular resolution is  $\sigma_\theta = 2.9^\circ$ , which was obtained by fitting  $N_0\theta \exp(-\theta^2/2\sigma_\theta^2)$  to the distribution.

The improvements in these kinematical variables are reflected to the improvements in the reconstructed  $W$  energies and directions as shown in Fig. 8a for the energy of the leptonically decayed  $W$ , Fig. 8b for the hadronically decayed  $W$ , and Fig. 8c for the direction of the leptonically decayed  $W$ . We can see dramatic improvements in all of these distributions, although the improvement in the direction of the hadronically decayed  $W$  is less dramatic. Both the energy resolution of the leptonically decayed  $W$  and hadronically decayed  $W$  are approximately 2.4 GeV, the angular resolution of the leptonically decayed  $W$  and hadronically decayed  $W$  are  $2.4^\circ$  and  $1.7^\circ$ , respectively.

Finally, we will examine the effects of the kinematical fit on the measurements of the direction and the magnitude of the top-quark momentum. In Fig. 9a,b, the difference of the reconstructed and generated directions of the  $t$  or  $\bar{t}$  quark is plotted against the generated top momentum, before and after the kinematical fit, respectively. We can see appreciable improvement by the fit. Nevertheless, since the top-quark direction becomes more and more difficult to measure as the top-quark momentum decreases, the resolution is still somewhat poor in the low momentum region. The angular resolution is largely determined by the reconstruction of the  $t$  or  $\bar{t}$  decayed into three jets. Remember that the resolution improvements were less significant for the hadronically decayed  $W$ , since the power of the constraints was used up mostly to recover the momentum information of the direct neutrino from the leptonically decayed  $W$  and the energy resolution for jets from the  $W$  was left essentially unimproved. The improvement in the measurements of the top-quark direction is mostly coming from the improvement in the  $b$

<sup>3</sup> This is in contrast with the result in [12], where a quite tight set of cuts was imposed upon the reconstructed  $W$  and  $t$  masses, and consequently their peak shifts were less apparent at the cost of significant loss of usable events. The goal of this study is to establish an analysis procedure to restore those events which would have been lost, by relaxing the tight cuts while keeping a reasonable accuracy for event reconstruction

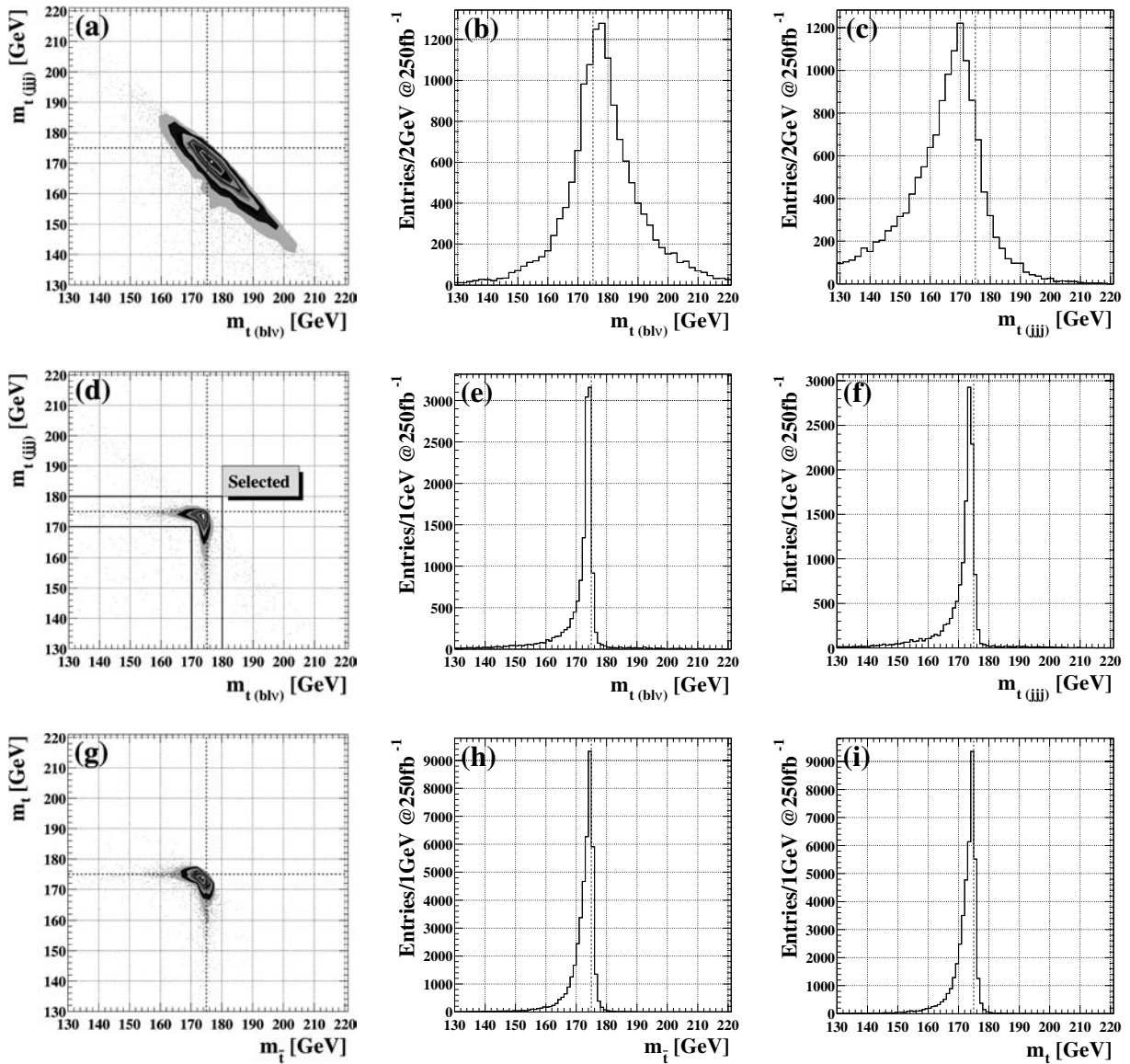


**Fig. 6a–i.** Scatter plot of the reconstructed  $t$  ( $\bar{t}$ ) mass from three jets versus that from a lepton plus a  $b$ -jet **a** before the kinematical fit, together with **b** its horizontal/ $bl\nu$  and **c** vertical/ $3$ -jet projections. **d** through **f** are similar plots after the kinematical fit and **g** through **i** are corresponding plots for generated values

or  $\bar{b}$  jet measurement. By the same token, the effect of the fit on the measurement of the magnitude of the top-quark momentum is also less dramatic compared to that on the leptonically decayed  $W$ . The momentum and angular resolutions of the  $t$  or  $\bar{t}$  quarks after the fit are approximately  $3.0\text{ GeV}$  and  $5.5^\circ$ , respectively.<sup>4</sup>

In the case of the 6-jet mode, for which there is no direct energetic neutrino from the  $W$ s, we can use the power of the constraints to improve the jet-energy measurements. Consequently, we may expect more significant improvement in the top-quark momentum measurement.

<sup>4</sup> Since the distributions deviate from Gaussian shapes substantially off their peaks, these values should be taken as order of magnitude estimates

## 5 A possible application

We discuss a possible application of our kinematical reconstruction method. Let us consider measurements of the decay form factors of the top-quark in the  $t\bar{t}$  threshold region. We assume that deviations of the top-decay form factors from the tree-level SM values are small and we consider the deviations only up to the first order, i.e. we neglect the terms quadratic in the anomalous form factors. Then the cross sections depend only on the two form factors  $f_1^L$  and  $f_2^R$  in the limit  $m_b \rightarrow 0$  although the most general  $tbW$  coupling includes six independent form factors [23]:

$$\Gamma_{Wtb}^\mu = -\frac{g_W}{\sqrt{2}} V_{tb} \bar{u}(p_b)$$



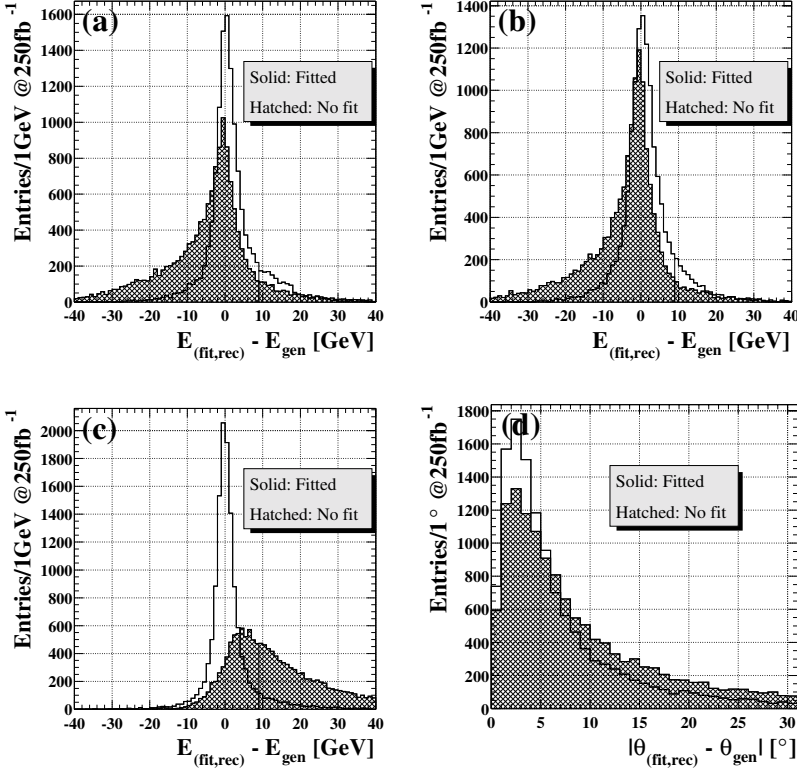


**Fig. 7a–d.** Distributions of the difference of the reconstructed and generated energies of the  $b$  or  $\bar{b}$  jet attached to **a** leptonically decayed and **b** hadronically decayed  $W$  bosons, together with the distribution of the difference of the reconstructed and generated  $c$  energies and **d** directions of the direct neutrino from the leptonically decayed  $W$ , before (*hatched*) and after (*solid*) the kinematical fit

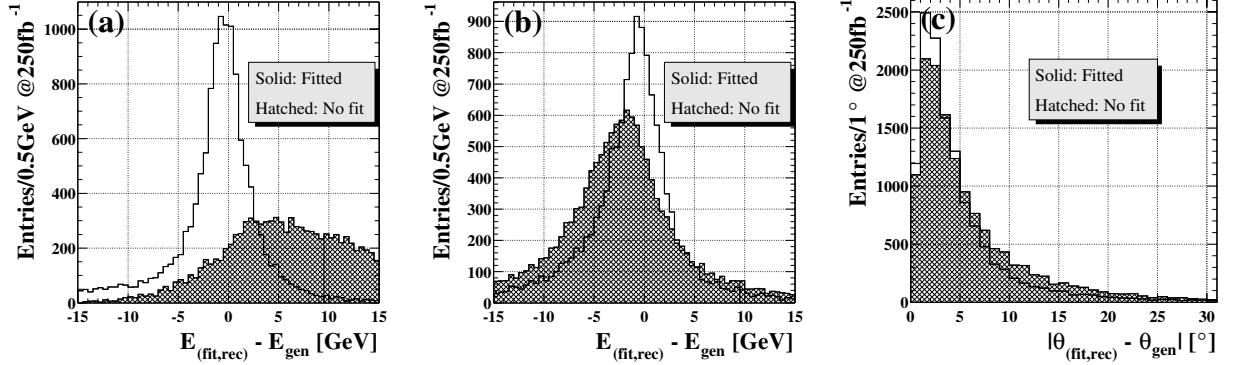


**Fig. 8a–c.** Distributions of the difference of the reconstructed and generated energies of **a** leptonically decayed and **b** hadronically decayed  $W$  bosons, and **c** distribution of the difference of the reconstructed and generated directions of the leptonically decayed  $W$ , before (*hatched*) and after (*solid*) the kinematical fit

$$\times \left[ \gamma^\mu f_1^L P_L - \frac{i\sigma^{\mu\nu} p_{W\nu}}{M_W} f_2^R P_R \right] u(p_t), \quad (2)$$

where  $P_L = (1 - \gamma_5)/2$  and  $P_R = (1 + \gamma_5)/2$ . At tree level of the SM,  $f_1^L = 1$  and  $f_2^R = 0$ . A variation of  $f_1^L$  changes only the normalization of the differential decay width of the top quark, whereas a variation of  $f_2^R$  changes both the normalization and the shape of the decay distributions. Thus we expect that the kinematical reconstruction is useful for disentanglement of the two form factors and in particular for the measurement of  $f_2^R$ . For simplicity we assume  $f_1^L = 1$  hereafter.<sup>5</sup> Since the transverse  $W$  (de-

noted as  $W_T$ ) is more sensitive to  $f_2^R$  than the longitudinal  $W$  ( $W_L$ ), our strategy is to extract  $W_T$  using the angular distribution of  $W$  (in the rest frame of  $t$ ) and the angular distribution of  $\ell$  (in the rest frame of  $W$ ). It is well known that  $W_T$  is enhanced in the backward region  $\cos \theta_W \simeq -1$ , where the angle  $\theta_W$  is measured from the direction of the top-quark spin in the  $t$  rest frame. Also, we may enhance  $W_T$  by collecting  $\ell$  emitted in the backward direction  $\cos \theta_\ell \simeq -1$ , where the angle  $\theta_\ell$  is measured from the direction of  $-\mathbf{p}_t$  in the  $W$  rest frame. These features are demonstrated in Fig. 10: We plot<sup>6</sup> (a) the differential decay width for the decay of the top quark with a definite spin orientation  $d\Gamma(t_\uparrow \rightarrow b\ell\nu)/(d\cos\theta_W d\cos\theta_\ell)$  for  $f_2^R = 0$  and (b)

<sup>5</sup> In order to determine  $f_1^L$  simultaneously, we may, for instance, use independent information from the measurement of the top width [12]

<sup>6</sup> We used the helicity amplitudes given in [23] for calculating these differential decay widths

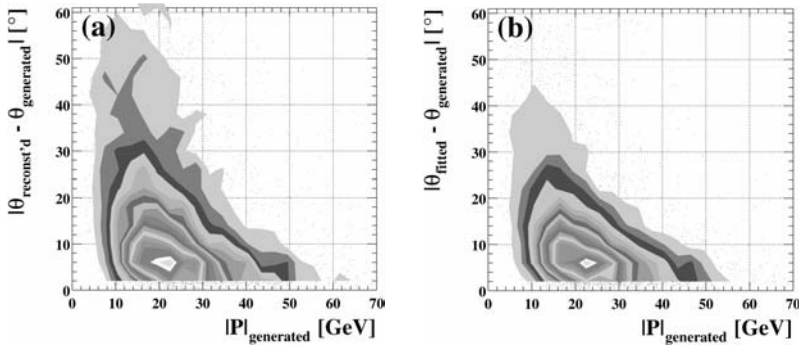


**Fig. 9a,b.** The difference of the reconstructed and generated directions of the  $t$  or  $\bar{t}$  quark plotted against the generated top momentum, **a** before and **b** after the kinematical fit

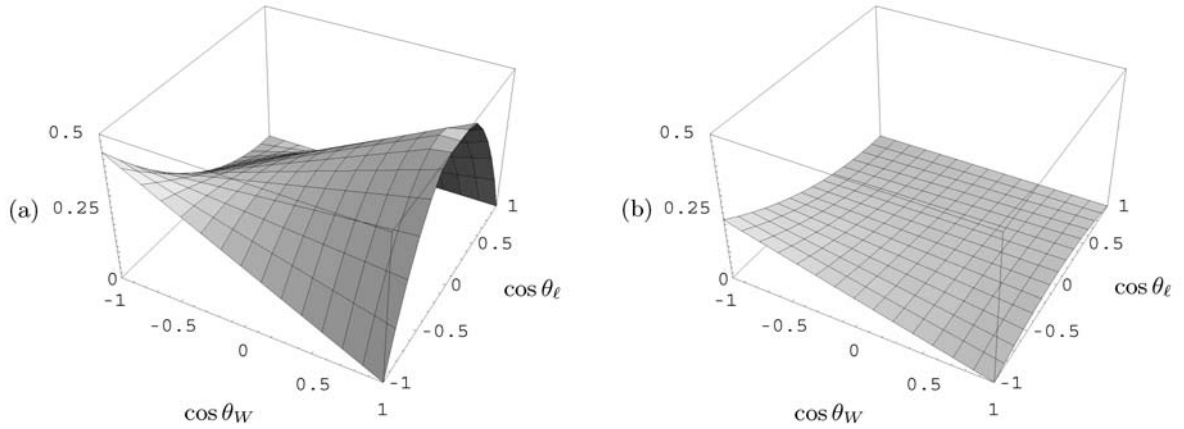


**Fig. 10a,b.** **a** Normalized differential decay width  $\mathcal{N}^{-1} d\Gamma(t_{\uparrow} \rightarrow b\ell\nu)/(d\cos\theta_W d\cos\theta_{\ell})$  for  $f_2^R = 0$ . **b** Difference of the normalized differential decay widths for  $f_2^R = 0.1$  and for  $f_2^R = 0$ . In both figures the differential widths are normalized by  $\mathcal{N} = \Gamma_t \times \text{Br}(W \rightarrow \ell\nu)$  for  $f_2^R = 0$

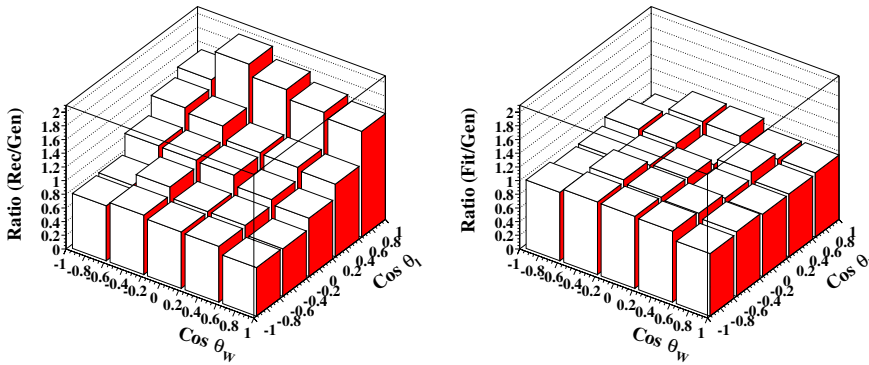


**Fig. 11a,b.** Reconstructed differential decay width distributions corresponding to Fig. 10a normalized by the generator-level distribution **a** before and **b** after the kinematical fit

the difference of the differential widths for  $f_2^R = 0.1$  and for  $f_2^R = 0$ . The plots show that we may measure  $f_2^R$ , for instance, from the ratio of the numbers of events in the regions  $\cos\theta_W, \cos\theta_{\ell} < 0$  and  $\cos\theta_W, \cos\theta_{\ell} > 0$ .

In the last section, we showed the significant improvement of the reconstruction of the leptonically decayed  $W$  due to the kinematical fit. In order to see how the improvement affects the measurement of the distribution in question, namely that in Fig. 10a, we compare the reconstructed and generated distributions before and after the kinematical fit, using the same Monte Carlo sample we used in the previous sections. Figure 11a,b plots, for the selected  $t\bar{t}$  sample, the reconstructed differential decay width normalized by the corresponding generator-level distribution before and after the kinematical fit. It is clear

from Fig. 11a that the measurement is biased towards high  $\cos\theta_{\ell}$ , which is because the energy of the leptonically decayed  $W$  tends to be overestimated so that the lepton from the  $W$  is often over-boosted. Figure 11b demonstrates that the kinematical fit effectively removed such a measurement bias. We expect therefore that the kinematical fit will reduce possible systematic errors in the differential width measurement significantly, thereby improving sensitivity to  $f_2^R$ .<sup>7</sup>

<sup>7</sup> We can extract  $f_2^R$  also from the distribution of  $\ell$  energies measured in the laboratory frame without relying on the reconstruction of its parent  $W$  momentum. The sensitivity of the lepton-energy distribution to  $f_2^R$  is, however, estimated to be lower than that of the differential decay width



It is advantageous to investigate the decay properties of the top quark in the  $t\bar{t}$  threshold region as compared to the open-top region  $E \gg 2m_t$  because of several reasons. First of all, the top quark can be polarized close to 100% in the threshold region [24,25], which is a useful tool to sort out various form factors. This is clear in the above example. Furthermore, we are almost in the rest frame of the top quark. In the above example, the top quark is highly polarized in its rest frame. Hence, the event rate expressed in terms of  $\cos\theta_W$  and  $\cos\theta_\ell$  is a direct measure of the amplitude-squared,  $|\sum_{i=L,T} \mathcal{A}(t_\uparrow \rightarrow bW_i) \times \mathcal{A}(W_i \rightarrow \ell\nu)|^2$  (without phase-space Jacobian), which allows for simple physical interpretations of the event shapes. We also note that we do not gain resolving power for the decay form factors by raising the c.m. energy. This is in contrast with the measurements of the  $t\bar{t}$  production form factors.

## 6 Summary and conclusions

To make maximum use of future  $e^+e^-$  linear colliders' experimental potential, the top-quark reconstruction in the lepton-plus-4-jet mode has been studied under realistic experimental conditions of the  $e^+e^- \rightarrow t\bar{t}$  process near its threshold. As a new technique to fully reconstruct the  $t\bar{t}$  final states, we have developed a kinematical fitting algorithm which aims to reconstruct the kinematical variables of top quarks and their offsprings more accurately.

The missing energy carried away by neutrinos from bottom quark decays has been recovered by the kinematical fitting. However, the effects of the kinematical fitting on the top-quark momentum are not as dramatic as we wanted. This is because the top quarks are almost at rest in the threshold region and therefore their momenta are difficult to measure. Moreover, in the lepton-plus-4-jet mode many constraints are used up by recovering the information on the neutrino from leptonically decayed  $W$  bosons. On the other hand, the remarkable improvements of the energy resolution of  $b$  jets and the angular and energy resolutions of leptonically decayed  $W$ s have been achieved by the kinematical fitting. These improvements should benefit the form factor measurements in general. As a possible application, we considered measurements of decay form factors including  $f_2^R$ , on which the correct reconstruction of the leptonically decayed  $W$  may have a large impact.

As stated in Sect. 1, many theoretical studies on measurements of the top form factors assumed either the most optimistic case or the most conservative case with respect to the kinematical reconstruction of event profiles. Our analysis indicates that both assumptions are not realistic under actual experimental conditions. In this respect we emphasize that the kinematical fit often took heavily skewed and broad distributions into nearly Gaussian shapes. Realistic phenomenological analyses using information of the decay particles from top quarks will then become possible by simply Gaussian smearing parton-level momenta with the resolutions for the measurements ob-

tained in this study. To be specific, the resolution for jet-energy measurements is  $\sigma_{E_j} \simeq 3.5$  GeV after the kinematical fit for both the light quark jets from  $W$ -boson decays and the bottom quark jets from  $t$  or  $\bar{t}$  quarks. As for the energy resolution for the neutrino coming from the leptonically decayed  $W$  we have  $\sigma_{E_\nu} \simeq 2.5$  GeV. The energy resolutions for both of the leptonically and hadronically decayed  $W$ s then become  $\sigma_{E_W} \simeq 2.4$  GeV, and the angular resolutions for the leptonically decayed  $W$  and the neutrino directly coming from it improve to  $2.4^\circ$  and  $2.9^\circ$ , respectively. Finally the momentum and angular resolutions for the  $t$  or  $\bar{t}$  quarks are approximately 3.0 GeV and  $5.5^\circ$ , respectively.

*Acknowledgements.* The authors wish to thank all the members of the ACFA working group for useful discussions and comments. In particular, they are grateful to S.D. Rindani for valuable discussions on strategies for measurements of top-quark's possible anomalous couplings, and A. Miyamoto for improving JSF (JLC Study Framework) to incorporate their requests. This work is partially supported by JSPS-CAS Scientific Cooperation Program under the Core University System and the Grant-in-Aid for Scientific Research No.12740130 and No.13135219 from the Japan Society for the Promotion of Science.

## References

1. F. Abe et al. [CDF Collaboration], Phys. Rev. Lett. **73**, 225 (1994); Phys. Rev. D **50**, 2966 (1994); Phys. Rev. Lett. **74**, 2626 (1995); S. Abachi et al. [D0 Collaboration], Phys. Rev. Lett. **74**, 2632 (1995)
2. JLC group, KEK Report, 92-16 (1992)
3. D. Atwood, S. Bar-Shalom, G. Eilam, A. Soni, Phys. Rept. **347**, 1 (2001)
4. ACFA LC working group, KEK Report, 01-11 (2001), hep-ph/0109166
5. J.A. Aguilar-Saavedra et al. [ECFA/DESY LC Physics Working Group Collaboration], hep-ph/0106315
6. T. Abe et al. [American Linear Collider Working Group Collaboration], in Proceedings of the APS/DPF/DPB Summer Study on the Future of Particle Physics (Snowmass 2001), edited by R. Davidson, C. Quigg, SLAC-R-570 Resource book for Snowmass 2001, 30 June-21 July 2001, Snowmass, Colorado
7. T.L. Barklow, C.R. Schmidt, in The Albuquerque Meeting (DPF94), edited by S. Seidel (World Scientific, 1995)
8. R. Frey, Proceedings of Workshop on Physics and Experiments with Linear colliders, Morioka-Appi, Japan, September (1995), hep-ph/9606201; R. Frey et al., hep-ph/9704243
9. M. Iwasaki [The Linear Collider Detector Group Collaboration], hep-ex/0102014; M. Iwasaki, hep-ex/9910065
10. S. Gusken, J.H. Kühn, P.M. Zerwas, Phys. Lett. B **155**, 185 (1985)
11. M. Peter, Y. Sumino, Phys. Rev. D **57**, 6912 (1998)
12. K. Fujii, T. Matsui, Y. Sumino, Phys. Rev. D **50**, 4341 (1994)

13. P. Comas, M. Martinez, R. Miquel, S. Orteu, M. Schmitt, Presented at 3rd Workshop on Physics and Experiments with  $e^+e^-$  Linear Colliders (LCWS95), Iwate, Japan, 8–12 September 1995
14. physsim-2001a, <http://www-jlc.kek.jp/subg/offl/physsim/>
15. H. Murayama, I. Watanabe, K. Hagiwara, KEK Report, 91-11 (1992)
16. S. Kawabata, *Comp. Phys. Commun.* **41**, 127 (1986)
17. Y. Sumino, K. Fujii, K. Hagiwara, H. Murayama, C.K. Ng, *Phys. Rev. D* **47**, 56 (1993)
18. H. Murayama, Y. Sumino, *Phys. Rev. D* **47**, 82 (1993)
19. T. Sjöstrand, *Comp. Phys. Commun.* **82**, 74 (1994)
20. S. Jadach, Z. Was, R. Decker, J.H. Kühn, *Comp. Phys. Commun.* **76**, 361 (1993)
21. JSF Quick Simulator, <http://www-jlc.kek.jp/subg/offl/jsf/>
22. S. Catani, Y.L. Dokshitzer, M. Olsson, G. Turnock, B.R. Webber, *Phys. Lett. B* **269**, 432 (1991); N. Brown, W.J. Stirling, *Z. Phys. C* **53**, 629 (1992)
23. G.L. Kane, G.A. Ladinsky, C.P. Yuan, *Phys. Rev. D* **45**, 124 (1992); G.A. Ladinsky, C.P. Yuan, *Phys. Rev. D* **49**, 4415 (1994)
24. R. Harlander, M. Jeżabek, J.H. Kühn, T. Teubner, *Phys. Lett. B* **346**, 137 (1995)
25. R. Harlander, M. Jeżabek, J. Kühn, M. Peter, *Z. Phys. C* **73**, 477 (1997)